The Electro-catalytic Desalination with CO_2 Reduction and O_2 Evolution

Kaixiang Shen[1,2], Qiang Wei[1,2], Xin Wang[1,2], Qiang Ru[1], Xianhua Hou[1*], Guannan Wang[3*], Kwan San Hui[4], Jiadong Shen[5], Kwun Nam Hui[6*], and Fuming Chen[1,2*]

[1] Guangdong Provincial Key Laboratory of Quantum Engineering and Quantum Materials, School of Physics and Telecommunication Engineering, South China Normal University, Guangzhou 510006, P.R. China, Email: houxianhua@m.scnu.edu.cn; fmchen@m.scnu.edu.cn

[2] School of Electronic and Information Engineering, South China Normal University, Foshan, 528225

[3] College of Medical Engineering& the Key Laboratory for Medical Functional Nanomaterials, Jining Medical University, Jining, 272067, China. Email: chemwangguannan@gmail.com

[4] Engineering, Faculty of Science, University of East Anglia, Norwich, UK

[5] School of Materials Science, South China University of Technology, Guangzhou 510641, P.R. China.

[6] Joint Key Laboratory of the Ministry of Education, Institute of Applied Physics and Materials Engineering, University of Macau, Avenida da Universidade, Taipa, Macau, PR China. Email: bizhui@umac.mo

Abstract: The electro-catalytic desalination with multi-functions is a promising method to increase the valued production of additional valuable chemicals during the desalination process. In this work, a multifunctional desalination device is demonstrated that can effectively desalinate the brackish water (15000 ppm) to 9 ppm while generating formate from captured CO_2 at Bi nanoparticle cathode and releasing oxygen at Ir/C anode. The salt feed channel is sandwiched between two electrode chambers and separated by ion exchange membranes. The electro-catalytic process accelerates the transportation of sodium ions and chloride ions in the brine to the cathode and anode chamber,

respectively. To date, the fastest salt removal rate is obtained, which can achieve up to 228.41 μg cm^{-2} min^{-1} with a removal efficiency of 99.94 %. The influences from the applied potential and the concentrations of salt feed & electrolyte are investigated in detail. The current research can provide a new route for the electrochemical desalination system.

Keywords: Electrochemical desalination; electrocatalytic desalination; CO_2 reduction; O_2 evolution, water rectification

Introduction

The shortage of fresh water is one of the crises that threaten sustainable development of society. Ocean is an unlimited water source, and seawater desalination is the unique solution to solve this crisis. In the last century, the scientists have been seeking various desalination methods to extract usable freshwater from the ocean. Among them, reverse osmosis and thermal distillation are the most mature, which dominate the percentage of 69 % and 25% in the global desalination capacity nowadays[1]. However, both the operation cost and the energy consumption are very high, and a lot of electrical or thermal energy must be consumed during the water treatment. For example, the electrical energy of 2-7 kWh m^{-3} is required for RO desalination, and the thermal distillation method consumes up to 15.5 kWh m^{-3} [1]. Capacitive deionization (CDI) is an economical and environmentally friendly desalination process, which remove the salt ions by the electrostatic absorption of the electric double layers on the surface of carbon electrodes [2-7]. However, the salt absorption capacity is very limited owing to low physical charge

storage capacitance[8]. It is suitable for the treatment application in a low concentration of salt feed, and the high salt content may cause the serious effect of co-ion repulsion[9, 10]. To improve the removal capacity, flow-electrode capacitive deionization (FCDI) was introduced [11, 12], which can achieve continuous treatment with an unlimited capacity[13-16]. The regeneration can be easily achieved by the mixture of the negative/positive electrode materials outside the device [14, 17]. The slow salt removal rate restricts its further development. Recently, the redox species or Faradaic electrode materials were employed in FCDI electrodes, which can improve the salt removal rate and reduce the energy consumption owing to the redox reaction [18-22]. Thus, the energy-saving desalination process can be achievable with the addition of redox couples in FCDI [23-25]. Up till now, most desalination devices were designed for a single desalination purpose. In 2018, Kim et. al. proposed a multi-functional desalination device. During the desalination, the chloride ion oxidation can effectively mediate the urea decomposition with titania electrocatalyst at anode [26, 27]. Meanwhile, hydrogen gas or carbon dioxide reduction is released with the electron acceptance from the outside circuit at the cathode. At the anode with the chloride oxidation, the generated hypochlorous acid may also de-gradate the membranes except for the urea decomposition[28], which may reduce the ion selectivity of ion exchange membrane and affect the sub-sequenced desalination process. So far, there are only a few studies on the electro-catalytic desalination [26, 27], and the electro-catalytic desalination with environment-friendly multi-functions and high removal rate & efficiency has not been achieved to date. As prospected by Prof. Choi[29], the multi-functional catalytic systems may possess a brighter future for energy- and resource-recovering water treatment. In this work, we demonstrate a novel three-in-one function

desalination device, including the simultaneous formate generation, the oxygen evolution and the salt removal. The device consists of bismuth catalyst for CO_2 reduction at the cathode chamber, a middle NaCl salt feed and Ir/C catalyst for the oxygen generation at the anode chamber. The three chambers are separated by a cation-exchange membrane (CEM) and an anion-exchange membrane (AEM), as shown in **Figure 1**. During the electro-catalytic desalination process, CO_2 is converted to formate with Na^+ migration into the catholyte through CEM. An oxygen evolution reaction occurs at anode chamber while Cl^- in the middle salt feed is transported to the anolyte stream via AEM. The results demonstrate that brackish water with 15000 ppm concentration can be desalted to 9 ppm, and the removal efficiency is up to 99.94%. The salt removal rate can be achieved up to 228.41 μg cm^{-2} min^{-1}, which is the best value to date. The influences of operating potential, concentrations of salt feed, and electrolyte concentration were investigated in detail. This novel desalination method not only achieves the ultra-high desalination performance but also provides the additional products of formate and oxygen, which may be significant on the application of electro-catalytic desalination.

Experimental section

Materials: Sodium bicarbonate ($NaHCO_3$, 99.8%) and sodium chloride (NaCl, 99.5%) were ordered from Shanghai Aladdin Biochemical Technology Co. The commercial bismuth nano-powder (Bi, 99.99%) and 20 wt% iridium on Vulcan XC-72 (Ir/C) was ordered from Shanghai Macklin Biochemical Co. and Premetek Co., respectively. These chemicals were directly used without any further treatment.

The electrode fabrication: The Bi working electrode is fabricated as follows: 8.0 mg of commercial Bi powder was dispersed in a solution containing isopropanol (500 μL) and 5 wt% Nafion solution (25 μL) with ultrasonic treatment for 30 min. Then, the as-prepared ink was dropped onto the hydrophobic carbon cloth (W1S1009, CeTech Co., Ltd) with the active size of 1.25 × 1.25 cm^2, and dried at 40 °C in the vacuum. The mass loading is 2.0 mg cm^{-2}. The Ir/C electrode was prepared below: 4.0 mg of Ir/C was dispersed in 1 mL isopropanol and 50 μL Nafion solution (5 wt%). A homogeneous ink can be formed after 30 minutes ultra-sonication, and was pasted on the carbon cloth as counter after drying in vacuum oven overnight.

The desalination device: The home-made desalination device was fabricated using the acrylic sheets and silica gel plates, as displayed in **Figure S1**. The Bi electrode and saturated calomel electrode were employed as the working and reference electrode in the cathodic compartment, respectively. The Ir/C electrode was used as the counter electrode in the anodic compartment. The desalination chamber was sandwiched using the cation exchange membrane (CEM) and anion exchange membrane (AEM). The three chambers are recirculated via the peristaltic pumps with the flow rate of 17 mL min^{-1}.

The electrochemical tests and the electro-catalytic desalination: The CHI 760E electrochemical workstation (CH Instruments, Inc, USA) was used for the electrochemical test. Linear sweep voltammetry (LSV) was recorded at the scan rate of 5 mV s^{-1}. In the electro-catalytic desalination tests, sodium bicarbonate with ~ 9 ml volume was chosen as both catholyte and anolyte. Before the electro-catalytic desalination, carbon dioxide was purged into the catholyte for 30 min and was continuously bubbled

with the flow rate of 30 sccm during the electro-catalytic desalination. The constant potential (-1.8V, -1.6V, -1.4V, -1.2V) was supplied by CHI 760E electrochemical workstation, and the current were synchronously recorded. The salt concentration was online monitored via the conductivity meter (eDAQ, EPU357). The 2 mL salt feed with the concentration of 4000, 8000, 12000, and 15000 ppm salt was used as the initial feeds. Three different concentration of sodium bicarbonate (0.1, 0.5, and 1.0 M) was employed to study the concentration influence of electrolyte.

Materials characterization and sample analysis: The powder X-Ray diffraction (XRD) patterns were performed on a PANalytical X'Pert PRO with Cu-Kα radiation at a scan rate of 10° min^{-1}. The microstructures of materials were obtained via the field emission scanning electron microscopy (FE-SEM; ZEISS ULTRA 55). The CO_2 reduction product, formate, was quantified by 1H nuclear magnetic resonance spectroscopy (NMR, Bruker AVANCE NEO 600 MHz). Typically, 600 μL CO_2 reduction electrolyte after desalination and 100 μL D_2O solution containing 0.05 μL of DMSO (used as the internal standard) was mixed as a measurement sample.

Results and discussions

The mechanism and performance of the electro-catalytical desalination

The schematic of the electro-catalytical desalination was shown in **Figure 1a** and the components in **Figure S1**. The commercial bismuth nanoparticles on the carbon cloth are used as the working electrode in 0.5 M sodium bicarbonate electrolyte. The CO_2 gas is

continuously bubbled into the electrolyte to maintain the saturation status, where most CO_2 is solvated[30]. The XRD pattern and SEM images of bismuth are displayed in **Figure S2**. The LSV measurements of Bi electrode were carried out in a typical three-electrode H-type cell with Pt counter and saturated calomel electrode (SCE) reference. As shown in **Figure S3**, the current density in CO_2 atmosphere is much higher than that in Argon, indicating the CO_2 reduction activity. Bismuth is regarded as an advanced catalyst for formic acid production because of its weak affinity for CO_2-intermediates and the low catalytical overpotential for CO_2 reduction reaction, which is beneficial to high energy efficiency and long-term stability[31]. In addition, Bi is low toxicity and harmless to the environment[32].

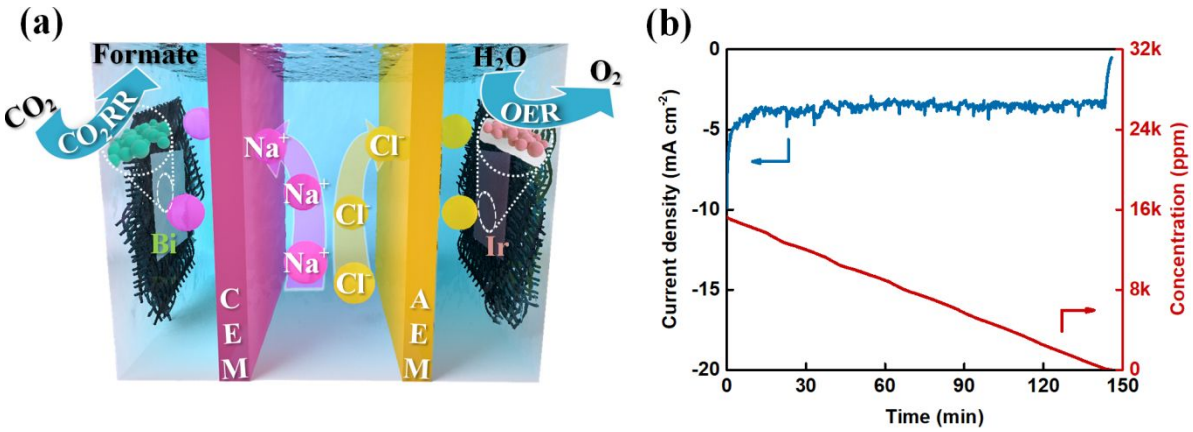

Figure 1. (a) Schematic of the multi-function electrocatalysis desalination. (b) The current density and desalination performance at the constant potential of -1.8V applied.

The bicarbonate has been regarded as proton donor in CO_2 reduction, because the HCO_3^- has smaller dissociation constants (pK_a) value than H_2O [33]. When CO_2 is continuously bubbled to catholyte and mainly dissolve into HCO_3^- [34]. The bicarbonate could release CO_2 molecules for CO_2 reduction and be regenerated from CO_2 in bulk solution in rapid equilibrium [35]. When the constant potential applied during the catalytical desalination in **Figure 1**, CO_2 is reduced to formate under Bi catalyst as displayed in equation (1) [32, 36, 37] . Simultaneously, the sodium ions in the middle salt feed will migrate to the catholyte stream through the CEM. The reaction process during CO_2 reduction can be presented as follow:

$$Na^+ + CO_2 + H^+ + 2e^- \rightarrow HCOO^-Na^+ \quad (1)$$

At the anolyte, the oxygen will be evolved with the Iridium catalyst as displayed in below equation (2) [38]. Meanwhile, the chloride ions in the middle salt feed will be transported to anolyte stream via AEM. In the anodic compartment, the Ir/C electrode was used as the electrocatalyst for oxygen evolution reaction (OER). The XRD spectra of Ir/C catalysis can be demonstrated in **Figure S4(a)**, which is assigned to metallic Ir (No. 03-065-9327). The SEM image shows an aggregation of spherical particles with size about 50 nm in **Figure S4(b)**. The overpotential of $\eta_{10\ mA\ cm-2}$ = 1.08 V vs. SCE can be achievable in the LSV curve in **Figure S5**. The reaction in anolyte can be demonstrated below:

$$4Cl^- + 2H_2O \rightarrow O_2 + 4HCl + 4e^- \quad (2)$$

The overall reaction is that formate can be formed from CO_2 reduction while the oxygen is released. The released electron during the oxygen evolution will travel to the working electrode for the CO_2 reduction process. To compensate for the static balance, the ions in the salt feed are removed to the anode and cathode chambers, and form the completed circuit. Thus, it is named the multi-function electrocatalysis desalination.

The performance of the electro-catalytical desalination is demonstrated in **Figure 1b**. When the constant potential of -1.8 V is applied, the current density can be maintained at the platform of ~3.62 mA cm^{-2}. The fluctuations of current density may be caused by the gas evolution, as shown in equation (2). The salt feed is continuously declined in **Figure 1b**, indicating a desalination process. The salt removal rate can reach 134.48 μg cm^{-2} min^{-1} with a charge efficiency of 91.11%. When the salt concentration in feed is 145 ppm at the last stage of desalination, the current density drops rapidly due to the insufficient salt ions inside, resulting in worse conductivity and huge resistance inside the device, as displayed in **Figure 1b** and **Figure S6**. At the end, 9 ppm water product can be achieved, which is the lowest level achieved in the electrochemical desalination to date. As known in the previous literatures[39], bismuth particles have the unique property for the CO_2 reduction reaction and the dominant reduction product is formate. Based on the results of the nuclear magnetic resonance spectroscopy, the liquid product formate is observed in **Figure S7**, which is consistent with the reaction equation (1). At the same time, the pH value shows a slightly downward trend due to the OH^- (mainly from the hydrolysis of bicarbonate) consumption, as displayed in **Figure S8**. Hence, the brackish water can be desalted to a few ppm product level in a one-step electro-catalytic desalination process,

and formate can be generated from CO_2 consumption at cathode and oxygen evolution at the anode during the charging process.

Desalination performance at the variation of the operating potential

The desalination performance of the electro-catalytic desalination is influenced by the operating potential. The potentials are supplied by the electrochemical working station with the range of -1.8 V to -1.2V, as shown in **Figure 2**. The time under each potential is controlled to 30 min, and the initial concentration of salt in feed is 12000 ppm. With the decreased potential, a lower current density is observed from -4.6 to -0.42 mA cm^{-2}. The slope of concentration change is also higher at the large potentials, as shown in **Figure S9**. The salt removal rate relies on the current density. In **Figure 2b**, the salt removal rates are 146.86, 91.54, 36.53, and 16.49 μg cm^{-2} min^{-1} at the potential of -1.8, -1.6, -1.4 and -1.2 V, respectively. The salt removal rate at -1.2 V is about 88.5% lower than that at -1.8 V. The rapid desalination process can be obtained at a higher potential.

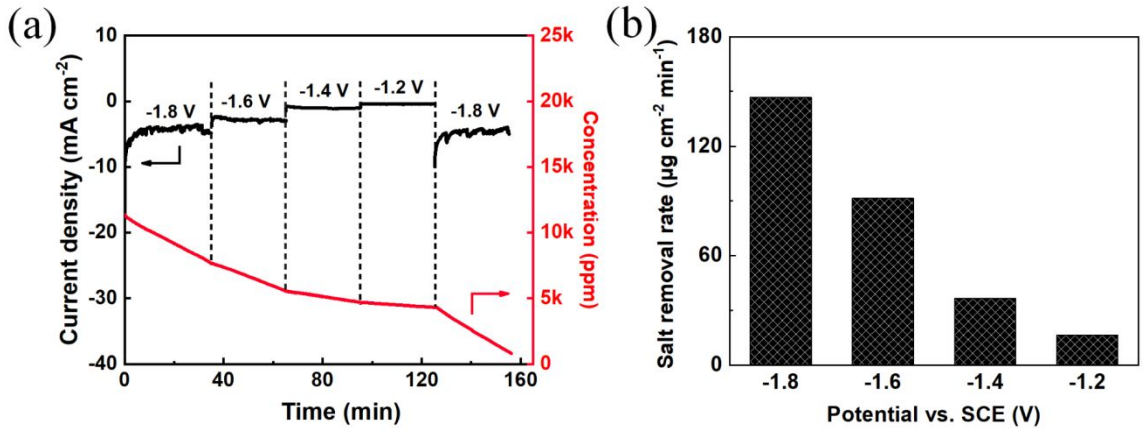

Figure 2. (a) The curves of current densities and salt concentration at the different applied potential, and the corresponding salt removal rate (b).

The effect from the salt feed concentration

The desalination performance influence from the initial salt concentration is further investigated in **Figure 3**. At a constant potential of -1.8V and a salt concentration in the range of 4000 to 15000 ppm, the current density does not change significantly. This may be due to the sufficient conductivity even in 4000 ppm salt feed. At the last stage of electro-catalytical desalination, the current density drops quite fast owing to the insufficient ion conductivity in the middle salt stream. **Figure 3a** demonstrates the concentration declination during the electro-catalytical desalination for all four different concentration tests. The K slope value has a negative correlation with the initial concentration of the salt feed. The lower salt removal rate is exhibited in the high concentration salt, and this may be attributed to the effect of Donnan potential and voltage drop of diluate solution in the high salt condition [40, 41]. This phenomena is also observed in the reported literature [42]. The corresponding salt removal rate is shown in

Figure 3b. For example, at the initial salt concentration of 4000 ppm, the salt removal rate can achieve up to 177.16 μg cm^{-2} min^{-1} under the operating potential of -1.8 V. However, the removal rate is low down 134.48 μg cm^{-2} min^{-1} when the initial concentration of salt feed is 15000 ppm.

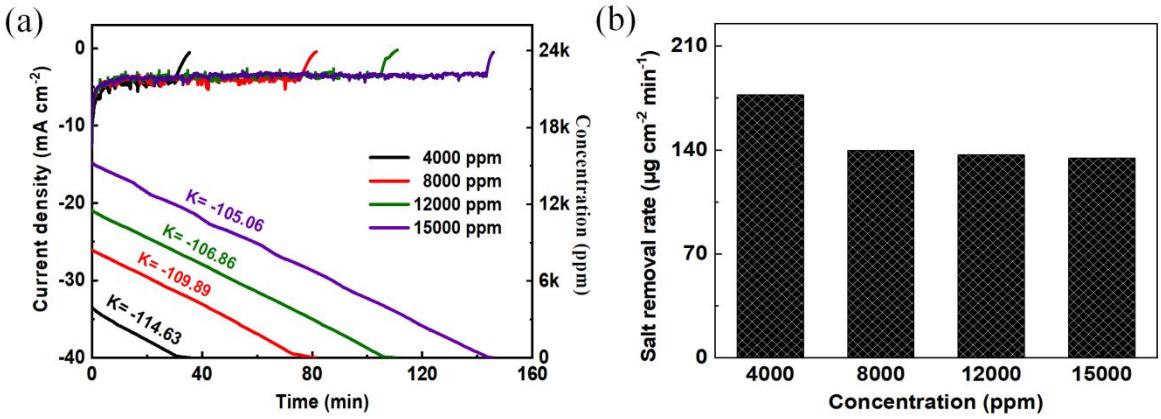

Figure 3. (a) The curves of current densities and salt concentration change at the different salt concentration at the operating potential of -1.8 V applied; and the corresponding salt removal rate (b).

The effect of electrolyte concentration

During CO_2 reduction reaction process, the partial CO_2 can be dissolved to form HCO_3^-. The proton release and $NaHCO_3$ concentration play an important role in the electrolysis on the surface of bismuth catalyst[35]. The high concentration of bicarbonate can provide more carbon dioxide to react and enhance the reaction current density. As displayed in **Figure 4**, the three different electrolyte concentrations are tested for comparison, i. e. 0.1, 0.5, and 1.0 M sodium bicarbonate. In **Figure 4a**, the maximum current density is

maintained up to 7.87 mA cm^{-2} in 1.0 M $NaHCO_3$ electrolyte at the operating potential of -1.8 V. The current values are directly proportional to the salt removal rate. As shown in **Figure 4b**, the slope of concentration change is three times higher in 1 M $NaHCO_3$ than that in 0.1 M concentration, indicating the quickest salt removal rate as displayed in **Figure 4c**. The maximum salt removal rate can reach up to 228.41 μg cm^{-2} min^{-1} at the condition of -1.8 V operating potential and 1.0 M $NaHCO_3$ electrolyte. **Figure S10** and **Table S1** exhibits the salt removal rate vs. year of publication for capacitive deionization (CDI), membrane capacitive deionization (MCDI), flow-electrode capacitive deionization (FCDI) and faradaic electrode desalination as well as the current electro-catalytic desalination. For the CDI (black diamond), the salt removal rate has risen from 0.99 to 142.86 μg cm^{-2} min^{-1} in two decades[43, 44]. The MCDI (green hexagon) system possesses a maximum salt absorption rate of 150 μg cm^{-2} min^{-1} (after 40 minutes of desalting)[45]. As for FCDI (purple dot), the salt removal rate reached 340 μg cm^{-2} min^{-1} in 35 g L^{-1} salt feed with at ~12% salt removal efficiency,[13] while under the ~92.7% salt removal efficiency, the salt removal rate was 162 μg cm^{-2} min^{-1} [18]. The high salt removal rate of faradaic electrode desalination (light blue triangle) can achieve 168.37 μg cm^{-2} min^{-1} [8]. For our electro-catalytic desalination system, the salt removal rate is high up to 228.41 μg cm^{-2} min^{-1} in the condition of -1.8 V operating potential. When the desalination process is completed, the salt removal efficiency is close to 100% with 9 ppm water product due to the high and stable current density. The current desalination process is driven by the electrical energy. In the future application, it could be integrated with solar energy or other alternative energy [46,47]

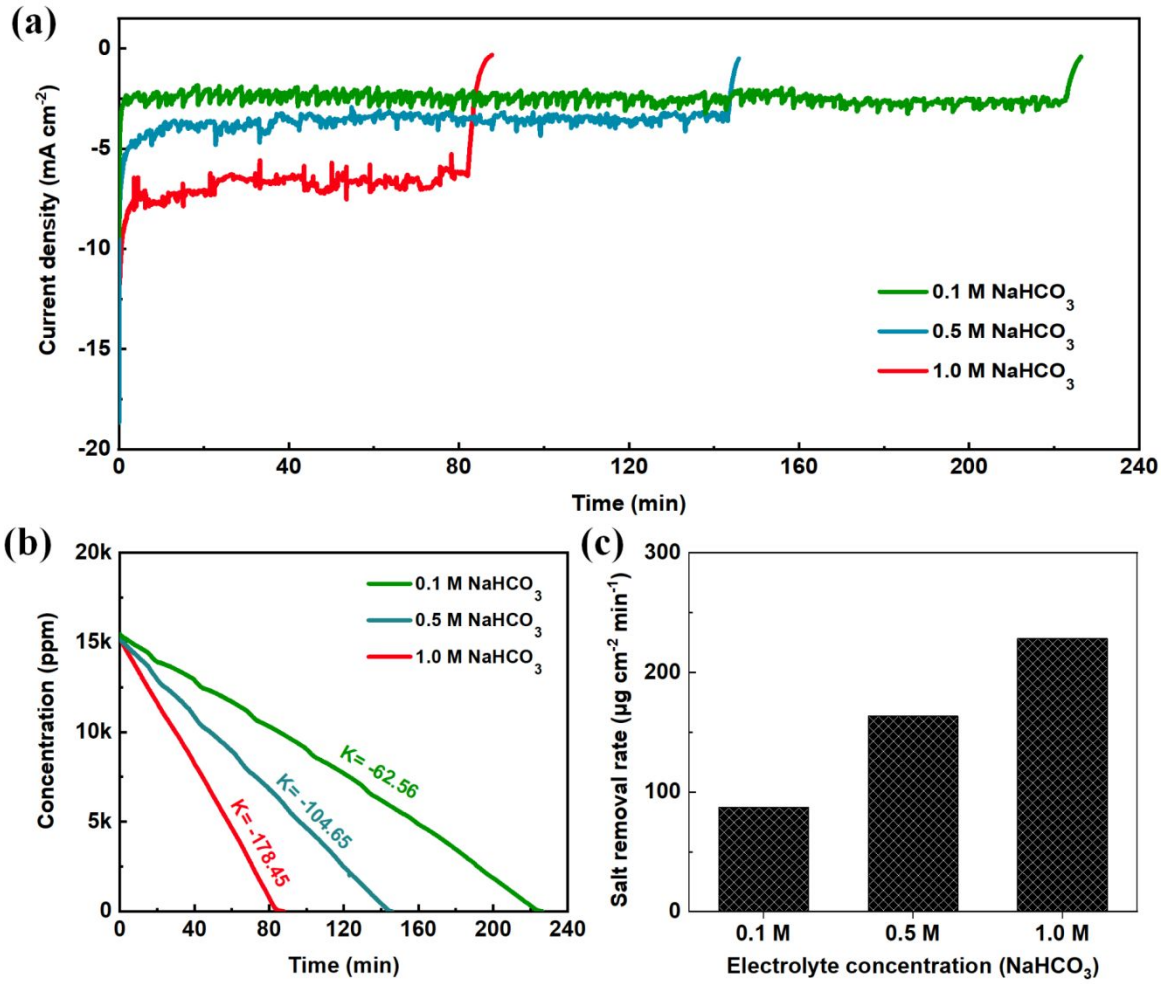

Figure 4. (a) The curves of current densities at the different concentration of $NaHCO_3$ electrolyte at the operating potential of -1.8 V applied; and the corresponding salt concentration change (b), and the salt removal rate (c) during the desalination. K is the slope of the simulated line.

Conclusion

The multi-function electrocatalysis desalination device is demonstrated that can simultaneously desalinate salt water to few-ppm level with formate formation from CO_2

consumption and oxygen evolution. The electro-catalytic desalination flow cell device can deliver a stable current density of ~3.62 mA cm^{-2} and the salt removal rate of 134.48 μg cm^{-2} min^{-1} in 0.5 M $NaHCO_3$ during the electrolysis desalination. When the concentration of $NaHCO_3$ electrolyte is raised to 1.0 M, the current density is raised to ~6.73 mA cm^{-2} at the operating potential of -1.8 V, and the maximum salt removal rate can reach up 228.41 μg cm^{-2} min^{-1}. As we know, these values of current density and removal rate are higher than most in the reported CDI, MCDI, FCDI, and Faradaic electrode desalination. The promising electro-catalytical behavior of electrode materials enables the fast electron transfer and ion movement, and causes the excellent desalination performance. The desalination performance is influenced by the applied potential, the concentration of salt feed and electrolyte, which will be further optimized in our future investigation. The electro-catalytical desalination will provide a novel view for the design of highly stable and fast desalination systems, and possesses significant guidance for the potential application.

Acknowledges

This project was supported by National Key Research and Development Program of China (2019YFE0198000), Science and Technology Program of Guangzhou (2019050001), National Natural Science Foundation of China (No. 81671742 & 51909165), Start-Up Grant of Jining Medical University (No. 600768001), Scientific and Technological Plan of Guangdong Province (2018A050506078), the Department of Education of Guangdong Province (2019KZDXM014), China Postdoctoral Science

Foundation (2020TQ0109, 2020M682753), SCNU Outstanding Young Scholar Project (8S0256), the Science and Technology Development Fund, Macau SAR (File no. 0191/2017/A3, 0041/2019/A1, 0046/2019/AFJ, 0021/2019/AIR), University of Macau (File no. MYRG2017-00216-FST and MYRG2018-00192-IAPME), and the UEA funding. F. Chen acknowledges the Pearl River Talent Program (2019QN01L951).

Conflict of Interest

The authors declare no conflict of interest.

References

1. K. Elsaid, M. Kamil, E. T. Sayed, M. A. Abdelkareem, T. Wilberforce and A. Olabi, *Sci Total Environ*, 2020, 748, 141528.

2. A. M. Johnson and J. Newman, *Journal of The Electrochemical Society*, 1971, 118, 510.

3. S. Evans and W. S. Hamilton, *Journal of The Electrochemical Society*, 1966, 113, 1314.

4. P. Srimuk, X. Su, J. Yoon, D. Aurbach and V. Presser, *Nature Reviews Materials*, 2020, 5, 517-538.

5. W. Tang, D. He, C. Zhang, P. Kovalsky and T. D. Waite, *Water Research*, 2017, 120, 229-237.

6. S. Vafakhah, M. Saeedikhani, M. Tanhaei, S. Huang, L. Guo, S. Y. Chiam and H. Y. Yang, *Nanoscale*, 2020, 12, 22917-22927.

7. D. Sriramulu and H. Y. Yang, *Nanoscale*, 2019, 11, 5896-5908.

8. F. Chen, Y. Huang, L. Guo, M. Ding and H. Y. Yang, *Nanoscale*, 2017, 9, 10101-10108.

9. C. Prehal, C. Koczwara, H. Amenitsch, V. Presser and O. Paris, *Nature Communications*, 2018, 9, 4145.

10. L. Guo, R. Mo, W. Shi, Y. Huang, Z. Y. Leong, M. Ding, F. Chen and H. Y. Yang, *Nanoscale*, 2017, 9, 13305-13312.

11. K. Luo, Q. Niu, Y. Zhu, B. Song, G. Zeng, W. Tang, S. Ye, J. Zhang, M. Duan and W. Xing, *Chemical Engineering Journal*, 2020, 389, 124051.

12. Y.-U. Shin, J. Lim, C. Boo and S. Hong, *Desalination*, 2021, 502, 114930.

13. S.-i. Jeon, H.-r. Park, J.-g. Yeo, S. Yang, C. H. Cho, M. H. Han and D. K. Kim, *Energy & Environmental Science*, 2013, 6, 1471-1475.

14. F. Yang, J. Ma, X. Zhang, X. Huang and P. Liang, *Water Research*, 2019, 164, 114904.

15. J. Ma, J. Ma, C. Zhang, J. Song, W. Dong and T. D. Waite, *Water Research*, 2020, 168, 115186.

16. W. Tang, J. Liang, D. He, J. Gong, L. Tang, Z. Liu, D. Wang and G. Zeng, *Water Research*, 2019, 150, 225-251.

17. P. Liang, X. Sun, Y. Bian, H. Zhang, X. Yang, Y. Jiang, P. Liu and X. Huang, *Desalination*, 2017, 420, 63-69.

18. Q. Wei, Y. Hu, J. Wang, Q. Ru, X. Hou, L. Zhao, D. Y. W. Yu, K. San Hui, D. Yan, K. N. Hui and F. Chen, *Carbon*, 2020, 170, 487-492.

19. F. Chen, Y. Huang, L. Guo, L. Sun, Y. Wang and H. Y. Yang, *Energy & Environmental Science*, 2017, 10, 2081-2089.

20. P. Srimuk, J. Lee, S. Fleischmann, S. Choudhury, N. Jäckel, M. Zeiger, C. Kim, M. Aslan and V. Presser, *J. Mater. Chem. A*, 2017, 5, 15640-15649.

21. F. Chen, J. Wang, C. Feng, J. Ma and T. David Waite, *Chemical Engineering Journal*, 2020, 401, 126111.

22. Z. Liu, W. Ma and H. Li, *Nanoscale*, 2020, 12, 7586-7594.

23. X. Hou, Q. Liang, X. Hu, Y. Zhou, Q. Ru, F. Chen and S. Hu, *Nanoscale*, 2018, 10, 12308-12314.

24. D. Desai, E. S. Beh, S. Sahu, V. Vedharathinam, Q. van Overmeere, C. F. de Lannoy, A. P. Jose, A. R. Völkel and J. B. Rivest, *ACS Energy Letters*, 2018, 3, 375-379.

25. Q. Liang, F. Chen, S. Wang, Q. Ru, Q. He, X. Hou, C.-y. Su and Y. Shi, *Energy Storage Materials*, 2019, 20, 203-207.

26. B.-j. Kim, G. Piao, S. Kim, S. Y. Yang, Y. Park, D. S. Han, H. K. Shon, M. R. Hoffmann and H. Park, *ACS Sustainable Chemistry & Engineering*, 2019, 7, 15320-15328.

27. S. Kim, G. Piao, D. S. Han, H. K. Shon and H. Park, *Energy & Environmental Science*, 2018, 11, 344-353.

28. J. De Paepe, L. De Pryck, A. R. D. Verliefde, K. Rabaey and P. Clauwaert, *Environmental Science & Technology*, 2020, 54, 3618-3627.

29. T. H. Jeon, M. S. Koo, H. Kim and W. Choi, *ACS Catalysis*, 2018, 8, 11542-11563.

30. Y. J. Sa, C. W. Lee, S. Y. Lee, J. Na, U. Lee and Y. J. Hwang, *Chemical Society Reviews*, 2020, 49, 6632-6665.

31. Y.-X. Duan, K.-H. Liu, Q. Zhang, J.-M. Yan and Q. Jiang, *Small Methods*, 2020, 4, 1900846.

32. X. Zhang, X. Sun, S.-X. Guo, A. M. Bond and J. Zhang, *Energy & Environmental Science*, 2019, 12, 1334-1340.

33. T. Li, C. Yang, J.-L. Luo and G. Zheng, *ACS Catalysis*, 2019, 9, 10440-10447.

34. H. Zhong, K. Fujii, Y. Nakano and F. Jin, *The Journal of Physical Chemistry C*, 2015, 119, 55-61.

35. X. Zhang, S.-X. Guo, K. A. Gandionco, A. M. Bond and J. Zhang, *Materials Today Advances*, 2020, 7, 100074.

36. K. Fan, Y. Jia, Y. Ji, P. Kuang, B. Zhu, X. Liu and J. Yu, *ACS Catalysis*, 2020, 10, 358-364.

37. J. Gu, F. Héroguel, J. Luterbacher and X. Hu, *Angewandte Chemie International Edition*, 2018, 57, 2943-2947.

38. Y. Dong, C. W. Oloman, E. L. Gyenge, J. Su and L. Chen, *Nanoscale*, 2020, 12, 9924-9934.

39. N. Han, Y. Wang, H. Yang, J. Deng, J. Wu, Y. Li and Y. Li, *Nature Communications*, 2018, 9, 1320.

40. N. A. A. Qasem, B. A. Qureshi and S. M. Zubair, *Desalination*, 2018, 441, 62-76.

41. S. K. Patel, M. Qin, W. S. Walker and M. Elimelech, *Environmental Science & Technology*, 2020, 54, 3663-3677.

42. J. Wang, Q. Zhang, F. Chen, X. Hou, Z. Tang, Y. Shi, P. Liang, D. Y. W. Yu, Q. He and L.-J. Li, *Journal of Materials Chemistry A*, 2019, 7, 13941-13947.

43. J. C. Farmer, D. V. Fix, G. V. Mack, R. W. Pekala and J. F. Poco, *Journal of The Electrochemical Society*, 1996, 143, 159-169.

44. T. Yan, B. Xu, J. Zhang, L. Shi and D. Zhang, *RSC Advances*, 2018, 8, 2490-2497.

45. H. Liu, J. Zhang, X. Xu and Q. Wang, *Chemistry – A European Journal*, 2020, 26, 4403-4409.

46. F. Chen, R. Karthick, Q. Zhang, J. Wang, M. Liang, J. Dai, X. Jiang and Y. Jiang, *Journal of Materials Chemistry A*, 2019, 7, 20169-20175.

47. J. Dai, M. Huang, K. S. Hui, D. Y. W. Yu, D. Yan, K. N. Hui, S. C. Tan, L. Zhang and F. Chen, *Chemical Engineering Journal*, 2021, 416, 127716.